Journal of Materials Chemistry B

PAPER

View Article Online
View Journal | View Issue

Cite this: J. Mater. Chem. B, 2025, 13, 5171

Light-activated spatiotemporal control over nanoreactor permeability†

Wouter P. van den Akker,[ab] Levena Gascoigne,[b] Alexander B. Cook,[a] Rolf A. T. M. van Benthem,[cd] Ilja K. Voets[b] and Jan C. M. van Hest*[a]

Received 13th October 2024,
Accepted 5th April 2025

DOI: 10.1039/d4tb02304h

rsc.li/materials-b

Interactive materials can be responsive to a variety of stimuli, such as pH, redox, or light. Actuation with light offers excellent spatiotemporal control. Furthermore, it has the advantage that no waste is produced during the light activation process. Herein, we present a strategy to regulate the permeability of pH-responsive nanoreactors using a spiropyran photoacid. Upon light illumination, the photoacid drastically reduced the pH of the environment, which caused the nanoreactor to become permeable. Encapsulation of an enzyme within these nanoreactors therefore allowed for light-induced enzymatic conversion of substrate, and longer irradiation times resulted in an increase in product. Additionally, apart from temporal control, we showed that immobilization of the nanoreactors into a hydrogel matrix also allowed for excellent spatial control. By using a photomask approach, we demonstrated that only in illuminated regions of the hydrogel substrate was converted, due to the local activation of the nanoreactors. Furthermore, this approach could also be applied with higher resolution using confocal microscopy. Irradiating targeted areas with a 480 nm laser line allowed for photoisomerization of the spiropyran, simultaneously inducing permeability. This approach yields high-resolution spatial control over nanoreactor permeability and could potentially be utilized in controlled local synthesis of products or drug release.

1. Introduction

Stimuli-responsive materials are a class of materials which are able to change their properties upon applying an (external) stimulus, such as pH, light, or temperature. However, their behavior is typically unidirectional: in order to revert the properties to their original configuration, a counter-trigger must be applied (acid–base *etc.*). To circumvent this, out-of-equilibrium and adaptive materials have gained significant interest over recent years.[1,2] Dissipative chemical reaction networks[3,4] and (pH$^-$) feedback systems[5–7] have been developed to increase system complexity and to overcome this unidirectionality. Apart from temporal control over material properties, spatial control is also an important key parameter for the development of next-generation materials with increased functionality.

Light is a non-invasive external stimulus, with the ability to obtain both high spatial and temporal control. Photocages, for example, have found much success in the activation of light-responsive molecules.[8–10] However, a significant disadvantage is the one-time use. A more reversible approach is the use of synthetic photoswitches. Commonly used classes of photoswitches include but are not limited to azobenzenes, spiropyrans, diarylethenes, and Donor–Acceptor Stenhouse adducts (DASAs).[11,12] These photoswitches undergo light-induced isomerization which is paired with a change in property, such as polarity, geometry, or dipole moment. These photoswitches have been used previously in self-assembly, controlled aggregation,[13,14] photopharmacology[15–17] and in controlling permeability in nanoreactors.[18,19] Typically, removal of the light stimulus results in the reversal of the material properties, as the photoswitch relaxes to its ground state, thereby giving the process a transient nature.

An elegant example is the light-controlled reversible aggregation of azobenzene functionalized gold nanoparticles by Klajn *et al.*[14] Upon irradiation with UV light, the azobenzenes isomerized into the *cis*-state, which was coupled by a large

[a] Department of Chemistry & Chemical Engineering, Institute for Complex Molecular Systems, Bio-Organic Chemistry, Eindhoven University of Technology, Helix, P.O. Box 513, 5600MB Eindhoven, The Netherlands. E-mail: j.c.m.v.hest@tue.nl
[b] Department of Chemistry & Chemical Engineering, Self-Organizing Soft Matter Eindhoven University of Technology, P.O. Box 513, 5600MB Eindhoven, The Netherlands
[c] Department of Chemistry & Chemical Engineering, Laboratory of Physical Chemistry. Eindhoven University of Technology, 5600MB Eindhoven, The Netherlands
[d] Shell Energy Transition Center Amsterdam, Grasweg 31, Amsterdam, 1031 HW, The Netherlands

† Electronic supplementary information (ESI) available. See DOI: https://doi.org/10.1039/d4tb02304h

increase in dipole moment, causing the nanoparticles to assemble into higher order, supraspherical assemblies which were visible by eye. In the absence of the UV trigger, these assemblies fell apart spontaneously over time. To demonstrate a potential application, images were created which were self-erasing. Furthermore, this process could be repeated multiple times.

Examples of photoswitchable nanoreactors are the DASA-polymersomes of Rifaie-Graham *et al.*[19] and the PEO-PSPA polymersomes of Wang *et al.*[18] In both cases, the photoresponsive molecule was incorporated within the hydrophobic portion of an amphiphilic polymer. These polymers were self-assembled into polymersomes, and upon irradiation, photoisomerization occurred which enabled the permeability of these nanoreactors. Wavelength selectivity was also obtained in the case of the DASA-polymersomes. Two distinct populations with different DASAs responding to either green or red light were utilized to control the enzymatic glucose oxidase–horse radish peroxidase (GOx–HRP) cascade reaction. When a mixture of these populations was irradiated with alternating cycles of red and green light, product was able to be formed over time.

An alternative approach is to exploit the photoacid properties of spiropyran/merocyanine species. Typically spiropyrans exist in the ring-closed form and, upon UV irradiation, open to the merocyanine form (and relax back to the ring-closed form in the dark). However modifications to the spiropyran structure can allow it to exist preferentially in the ring-open merocyanine (MCH) form in aqueous conditions. Upon light illumination, the MCH photoisomerizes into the ring-closed spiropyran (SP), releasing a proton in the process which results in the acidification of the medium. The pH-switching regime is highly dependent on the pK_a of the merocyanine. Modification of the conjugated system by either electron-donating or electron-withdrawing groups allows for careful tuning of the desired pK_a and therefore the pH-regime of interest. Moreover, such modifications also shift the λ_{max} of the specific analog. Previous research has shown a large variety in merocyanine analogs, each with its distinct pK_a, and reported pH jumps as large as 3.5 pH points.[20–22] The spiropyran photoacid approach has been employed for the (self-)assembly of nanoparticles or fibers,[23–26] the formation of (patterned) supramolecular hydrogels,[27] light-controlled DNA binding,[28] but also the light-induced permeability switch of pH-responsive nanoreactors.[29]

We have previously shown the effectiveness of our pH-responsive bicontinuous nanospheres (BCNs), whose permeability could be switched by adjusting the pH of the solution utilizing the urease-feedback loop.[30] At neutral pH, the enzyme-loaded nanoreactors are impermeable to the substrate, and upon acidification of the medium, the nanoreactors become permeable which allows for enzymatic conversion of the substrate. Here, we present an approach to achieve spatiotemporal control over nanoreactor permeability induced by a light stimulus. To achieve this, we employed the photoacid merocyanine in combination with our previously developed pH-responsive nanoreactors. Upon isomerization of the photoacid, the pH dropped significantly, which consequently enabled the permeability of the nanoreactors. We translated this behavior into a hydrogel matrix, in which the nanoreactors were immobilized. Selective irradiation of targeted areas resulted in the local activation of the permeability of the enzyme-loaded BCNs, which gives spatial control in addition to temporal control.

2. Results and discussion

Fig. 1 shows the design to induce a light-responsive permeability switch in pH-responsive nanoreactors. Photoisomerization of the photoacid causes a significant change in pH. In response, the pH-responsive nanoreactors can change their permeability state, which is quickly reversed by the removal of the light stimulus. The BCN nanoreactors were constructed following earlier reported procedures using as polymer mPEG$_{45}$-*b*-p[DEAEMA$_{175}$-*co*-BMA$_{28}$] comprising pH-responsive 2-(diethylamino)ethyl methacrylate (DEAEMA) and 4-(methacryloyloxy) benzophenone (BMA) as hydrophobic block.[30] The BCNs were assembled using the nanoprecipitation method. The nanoparticles were photocrosslinked (utilizing the photoactivatable benzophenone) to prevent dissociation at low pHs. Consequently, acidification resulted in the swelling of the BCNs and made them permeable. Previous experiments with BCNs indicated that the pH at which the nanoreactors became impermeable was approximately pH 7.5, which coincided with the pH-dependent size switch as measured by DLS pH-titrations.[30] For this reason, we opted to use the methoxy-substituted spiropyran analog **1**, whose pK_a (7.4) was most compatible with our pH-responsive BCNs and would span the pH regime of interest. Compound **1** was synthesized according to previously published literature.[21,22] The characterization of the BCNs by dynamic light scattering is shown in Fig. S7 (ESI†).

Since the pK_a of **1** was most suitable for the light-induced permeability switch of the pH-responsive nanoreactors, we investigated its properties in greater detail. Fig. 2A shows the recovery of the photoswitch after illumination using UV-vis spectroscopy. The characteristic absorbance band quickly recovered, indicating the relaxation towards the ring-open merocyanine in the dark. Next, we investigated the photoacid properties. Initially, 0.5 mM of **1** (neutralization factor α = 1) was continuously irradiated using a 470 nm blue light LED (32 mW) until the pH reached its minimum ($\sim$pH 4). The light source was switched off and the pH recovery over time was measured. The measured pH jump spanned a pH window of $\sim$3.2. This was repeated for at least 3 cycles without observing any fatigue, as illustrated in Fig. 2B.

We also investigated the influence of neutralization factor α, which is the total equivalents base added to the system, compared to MCH. This increases the solubility of MCH as well as initial solution pH. The addition of small amounts of base shifts the pH of the solution in the dark towards the pK_a of the MCH, which allows for larger pH jumps upon light irradiation. Fig. S8A (ESI†) shows that with increasing α larger pH-jumps were achieved, as an α = 0 resulted in a pH-jump of $\sim$2.5 whereas increasing α to 1 resulted in a pH-switch of 3.2. The bottom plateau was not significantly influenced by α.

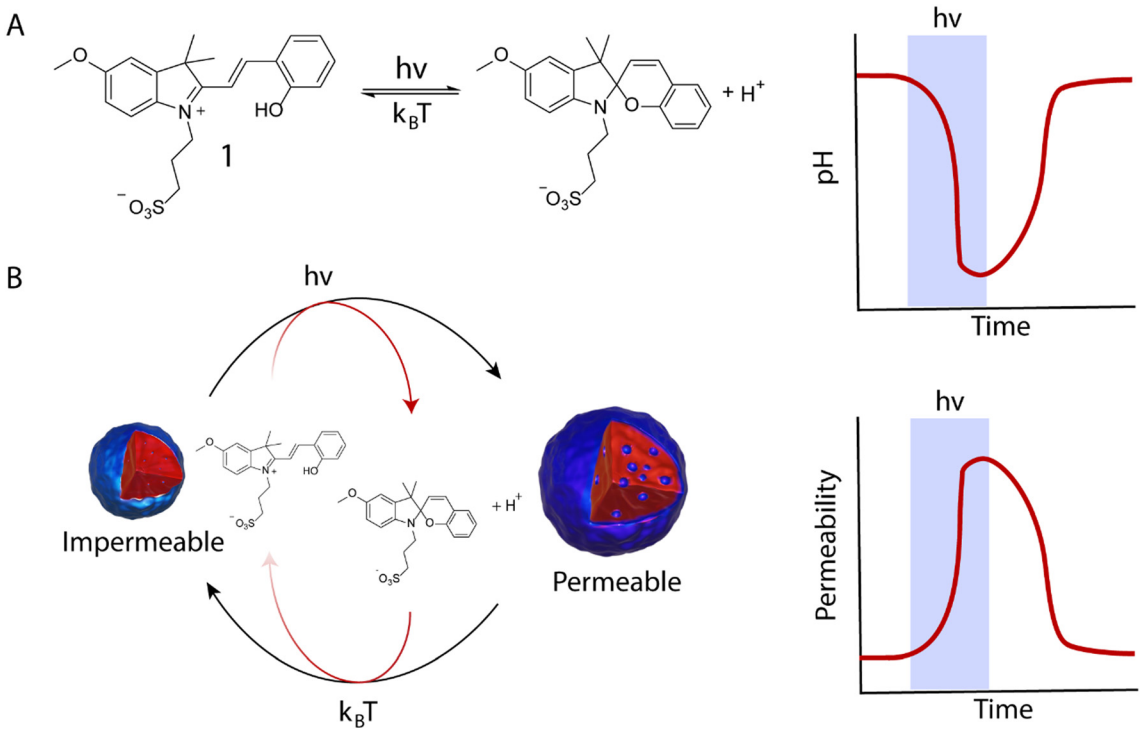

Fig. 1 Schematic illustration of the light-induced permeability switch. (A) Spiropyran photoacid **1** is utilized for the (reversible) light-triggered pH change. (B) pH-responsive nanoreactors are used in conjunction with the spiropyran photoacid to obtain a light-responsive permeability switch.

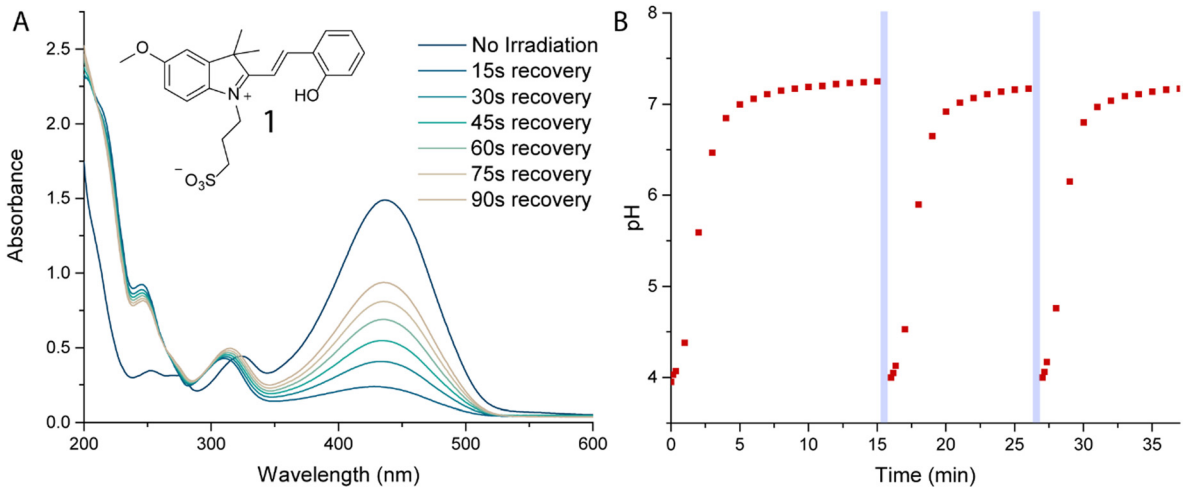

Fig. 2 (A) Relaxation of **1** measured by UV-vis spectroscopy. (B) Light induced pH switching of **1**. This is reversible for at least 3 cycles. Blue bars indicate irradiation. Experimental conditions: α = 1, 10 mM NaCl. [**1**] = 0.5 mM.

These results are in line with previous reports.[12] Apart from α, another key parameter in the photoswitching behavior is the light intensity. Laser powers of 32 mW & 16 mW were effective in decreasing the pH towards pH 4, however, at lower powers, such as 8 mW and 4 mW, the light intensity was not sufficient to fully push the equilibrium towards the ring-closed spiropyran, resulting in a lower pH drop upon illumination (Fig. S8B, ESI†).

Next, the influence of buffer capacity on the switching behavior of **1** was investigated. High buffer capacities naturally diminish the effect of the pH-switch, as the buffer would compensate for the proton release. For this purpose, we varied the ratio of [phosphate buffer] and [**1**] between 1 : 5, 1 : 1 and 2 : 1. At a low buffer capacity of 0.1 mM (1 : 5 ratio) we could still effectively switch the pH from ~4 to 6.8. However, at a 1 : 1 ratio, the pH-switching became significantly less effective, and a pH-switch from 6.4–7 was observed. Finally, increasing the buffer capacity to twice the concentration of [**1**] resulted in an ineffective pH switch, indicating that the buffer fully diminished the effect (Fig. S9A, ESI†).

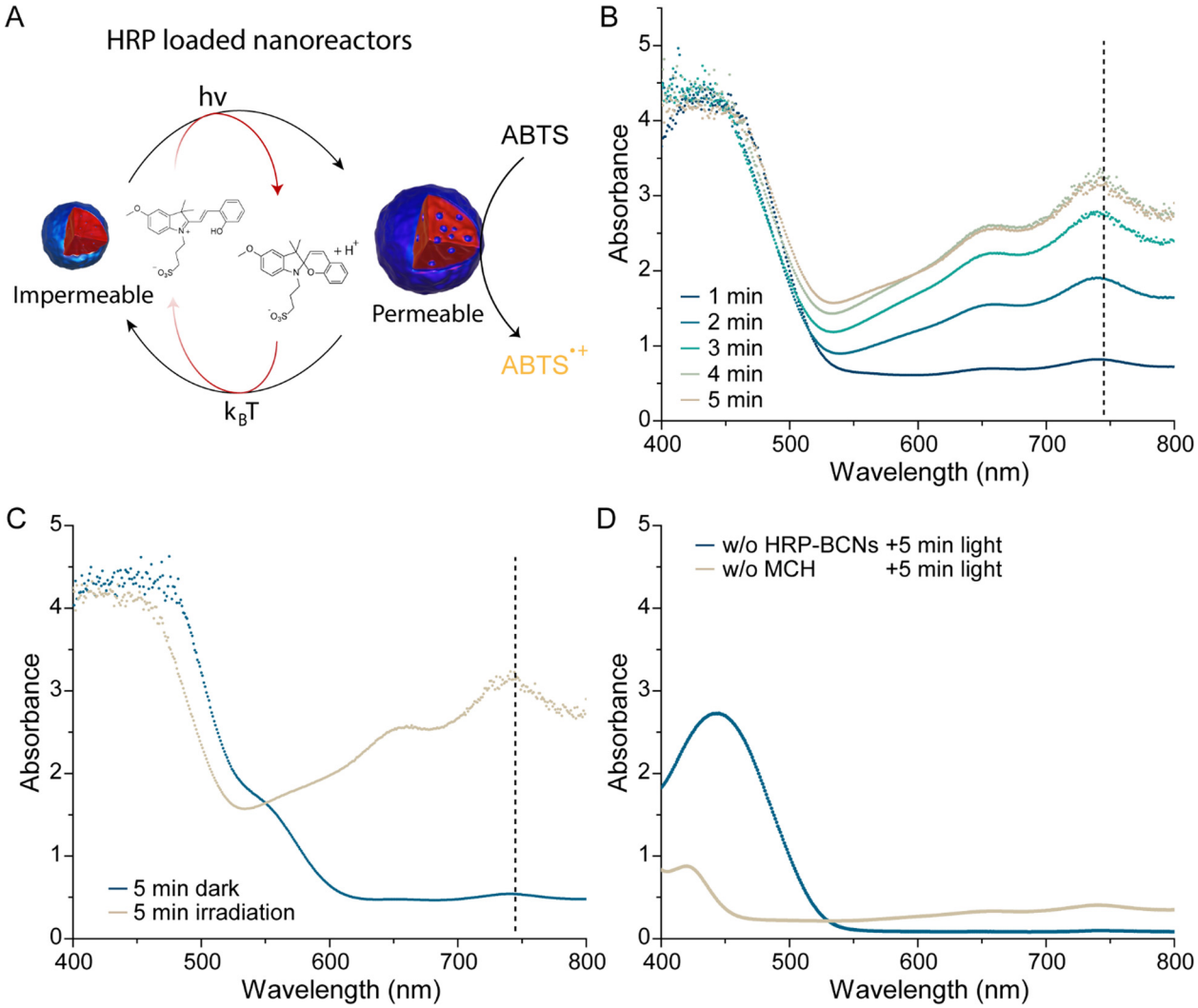

Fig. 3 (A) Light-induced permeability switch of pH-responsive BCNs. (B) Increasing irradiation times result in increased conversion of ABTS. (C) Comparison of non-irradiated HRP-BCNs with irradiated HRP-BCNs, both in presence of substrate. (D) Additional controls indicating that both MCH and HRP-BCNs are required for significant conversion of ABTS. Experimental conditions: 25 μg mL^{-1} BCNs, 0.5 mM [**1**], 10 mM NaCl, 2 mM $ABTS^{*+}$, 1 mM H_2O_2.

Since the nanoreactors are pH-responsive, they are also able to buffer the pH-switching to some extent. We therefore investigated whether the BCNs influenced the pH-switching behavior. Indeed, at higher BCN concentrations (500 μg mL^{-1}) the system was unable to change its pH upon illumination (Fig. S9B, ESI†). By decreasing the BCN concentration to 100 μg mL^{-1} we were once again able to alter the pH. However, the pH recovery profile was significantly slower in comparison to free merocyanine. Further decreasing the nanoreactor concentration towards 25 μg mL^{-1} resulted in a near-identical pH-recovery in comparison to MCH-only conditions. To guarantee efficient photoswitch behavior, we opted to use 25 μg mL^{-1} nanoreactor concentrations for subsequent experiments.

To investigate the light-induced permeability switch, we opted to encapsulate the enzyme horse radish peroxidase (HRP) in the BCNs, which converts the substrate ABTS into $ABTS^{*+}$ in the presence of H_2O_2 (Scheme S1, ESI†). HRP was encapsulated by dissolving it in the aqueous solution (1 mg mL^{-1}) before self-assembly, during which the polymer in THF was slowly added to the enzyme solution. The formed nanoreactors were then crosslinked for 5 minutes by UV irradiation and purified using dialysis and spin filtration to remove THF and non-encapsulated enzymes. The BCNs (25 μg mL^{-1}) were then mixed with 0.5 mM of **1**, 2 mM ABTS and 1 mM H_2O_2. Upon illumination, the pH decreased and the nanoreactors became permeable, significantly enhancing the catalytic output of the enzyme, as schematically depicted in Fig. 3A. By varying the irradiation times of the nanoreactors we were able to achieve different conversions of the ABTS substrate, as illustrated in Fig. 3B, by monitoring the multiple characteristic absorbance bands of $ABTS^{*+}$ at 415, 660 and 730 nm wavelengths. At longer irradiation times the absorbance plateaued, implying ineffective light absorption of the MCH due to the spectral overlap with the 415 nm peak of $ABTS^{*+}$, which would render the MCH

unable to switch, and therefore unable to acidify the solution. Furthermore, the amount of substrate converted while the sample was kept in the dark for 5 minutes was very low (Fig. 3C). Additional controls were done in the absence of the HRP-loaded BCNs and the absence of MCH and it was found that having both present under illumination is necessary for significant conversion. In the absence of MCH, some background conversion of ABTS was observed, while the absence of HRP-BCNs resulted in no conversion at all, indicating that the employed experimental conditions did not cause photooxidation of the substrate (Fig. 3D).

To gain spatial control over the nanoreactor activation, the HRP-loaded BCNs were immobilized within a hydrogel matrix (Fig. 4A). For this purpose, a 10 wt% acrylamide (AAm) hydrogel using *N*,*N*′-methylenebisacrylamide (MBA) as crosslinker (50 : 1 AAm : MBA) was synthesized using lithium phenyl-2,4,6-trimethylbenzoylphosphinate (LAP) as photoinitiator. The BCNs and the merocyanine **1** were dispersed in the monomer solution before the photopolymerization step. The hydrogels were synthesized by dispersing 100 μL of the monomer solution into transparent 96-well plates before photopolymerization for 6 minutes using a UV chamber with a power of 5 mW cm^{-2} at λ = 365 nm. The amount of merocyanine **1** was identical (0.5 mM) to the experiments performed in aqueous conditions. Fig. 4B shows that the recovery time increased quite significantly when the MCH was in a hydrogel compared to aqueous conditions. Fig. 4C shows representative snapshots of an MCH-hydrogel immediately after irradiation (0 min) and after recovery times of 5 and 10 minutes, clearly showing the recovery of the colored merocyanine species.

Irradiation of the immobilized HRP-BCNs in the presence of ABTS substrate for 5 minutes showed the formation of the characteristic absorbance bands of $ABTS^{*+}$ at 660 and 730 nm while keeping the hydrogel in the dark resulted in no significant conversion (Fig. 4D). Continuous UV-vis monitoring of non-illuminated hydrogels showed very limited conversion over a time-span of 5 minutes (Fig. S10, ESI†), indicating that the background permeability, and thus enzymatic conversion, is low. Quantification of the enzymatic conversion showed a >20-fold increase in substrate conversion when the nanoreactors were exposed to light in comparison to non-irradiated samples, indicating that the light-induced permeability switch was fully functional within the hydrogel environment.

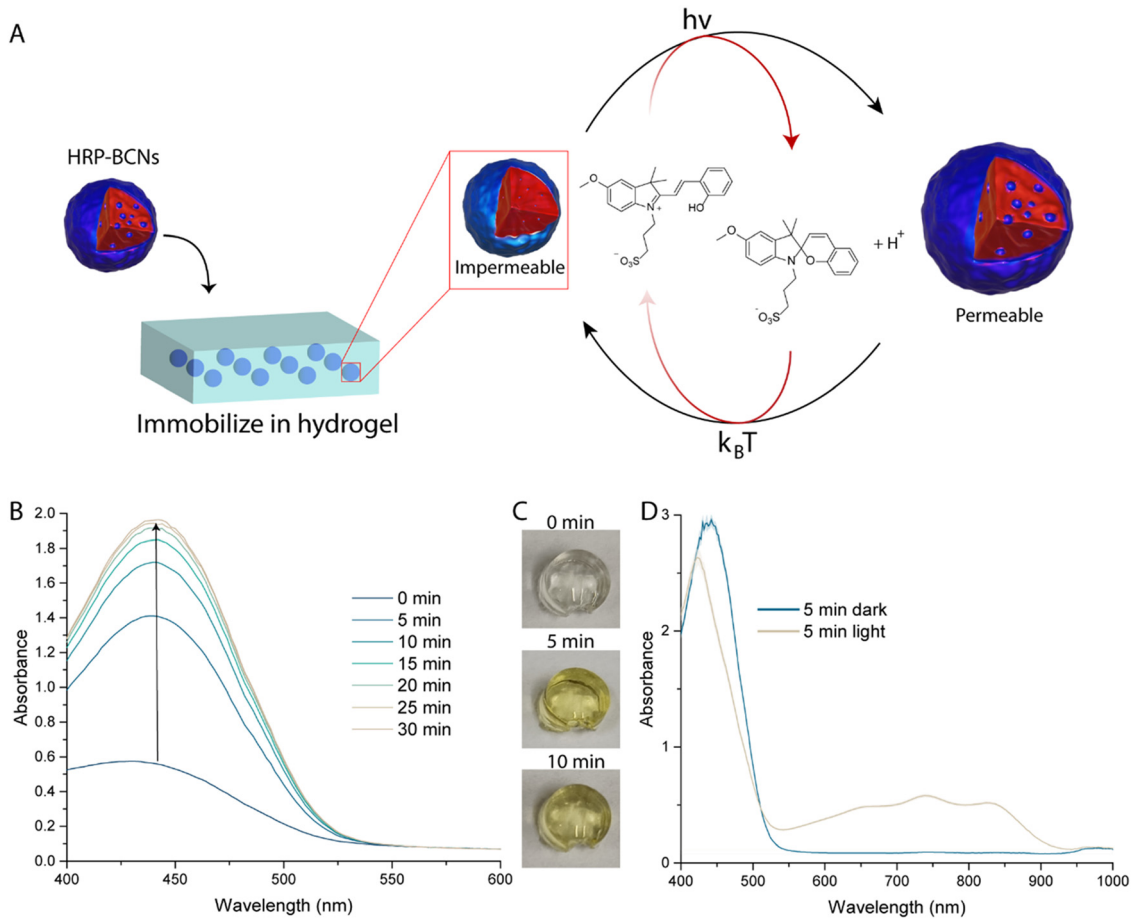

Fig. 4 (A) Immobilization of HRP loaded BCNs into a hydrogel matrix. (B) UV-vis spectroscopic analysis of merocyanine recovery within the hydrogel. (C) Corresponding snapshots of merocyanine recovery in an irradiated hydrogel. (D) Light-induced permeability switch of BCNs embedded in the hydrogel. Experimental conditions: 25 μg mL^{-1} BCNs, 0.5 mM [**1**], 10 mM NaCl, 2 mM ABTS, 1 mM H_2O_2. 10 wt% acrylamide hydrogel (50 : 1 AAm : MBA).

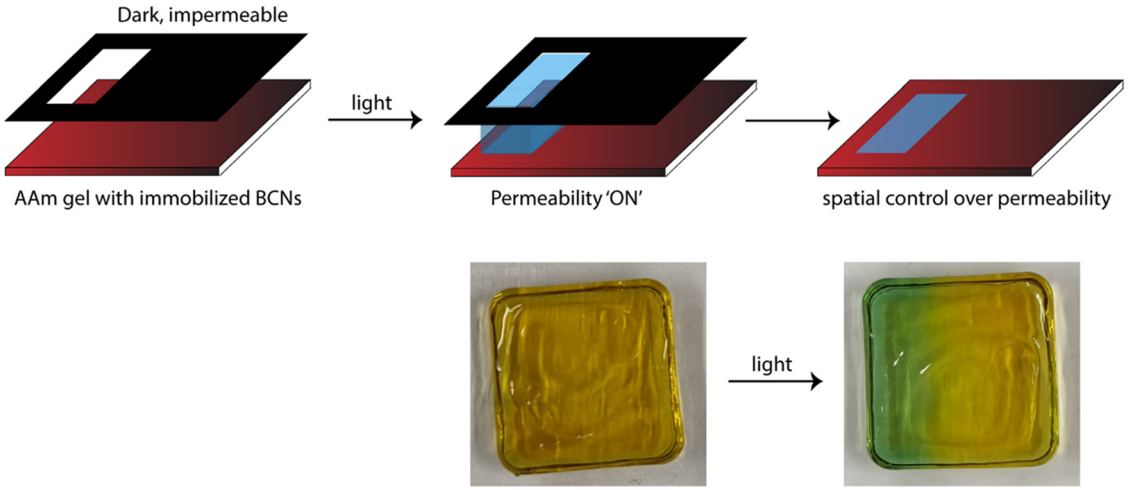

Fig. 5 Spatiotemporal control over nanoreactor permeability. Partial irradiation of a hydrogel caused product formation specifically at the illumination site.

We subsequently investigated the ability to obtain spatiotemporal control over nanoreactor activity. For this purpose, we synthesized a hydrogel with 1 × 1 cm dimensions by photopolymerization of the monomer solution containing **1** and HRP-loaded nanoreactors in a designated mold. The hydrogel was immersed in a 2 mM ABTS and 1 mM H_2O_2 solution for 30 minutes and then washed and dried to remove any liquid substrate present. As proof of concept, we irradiated about 1/3 of the hydrogel area and covered the other segment utilizing a photomasking approach. After 5 minutes of irradiation, we observed a significant color change due to ABTS conversion at the irradiated area, as illustrated in Fig. 5. This emphasized that using this approach, we can achieve both spatial and temporal control over nanoreactor permeability.

Furthermore, we tested whether we could utilize confocal & brightfield microscopy to obtain spatial control, as this may achieve higher resolution and prevent the need for photomasks. We utilized the microscope 480 nm laser line at maximum intensity to switch the merocyanine to the spiropyran and configured the microscope to monitor the RGB-transmission channels, whose wavelengths are centered at 660 (R), 520 (G), and 450 nm (B). In this instance, we irradiated an area of ~1.8 mm in diameter. After irradiation, the merocyanine absorbance band decreased, which correlates to an increased transmission of the blue channel. This increased transmission decreased over time as the spiropyran isomerized back to the merocyanine, but also due to diffusion (Fig. 6A). Without the addition of the ABTS substrate, the red channel signal remained constant as there was no change in absorbance because no product was formed (Fig. S11, ESI†). However, when the hydrogel was soaked in the substrate, at the irradiation spot ABTS was converted into $ABTS^{\bullet+}$ which yielded an increase in absorbance, and thus a decrease in red channel transmission. When a specific area with a radius of ~3 mm was bleached, we observed a simultaneous, overlapping increase in the blue channel transmission and a decrease in red channel transmission, indicating that the nanoreactors were spatially activated. It must be noted that during irradiation product could diffuse in three dimensions.

These results show that we can obtain spatiotemporal control over nanoreactor permeability by immobilization of these nanoreactors into a hydrogel matrix. Furthermore, the use of confocal laser lines showcases the broad applicability of the system, and allows for careful spatial selection over permeability, which could be utilized for local product synthesis or cargo release. In general, the resolution is somewhat limited by diffusion of both acid and product through the gel. We achieved a resolution with the photomask of around 2 mm, and with the confocal of 0.5–1 mm.

3. Conclusions

In this work we presented an approach to achieve both spatial and temporal control over nanoreactor permeability using light as external stimulus. We utilized previously developed pH-responsive bicontinuous nanospheres whose permeability can be switched 'ON' in acidic conditions and switched 'OFF' in neutral conditions. Pairing these pH-responsive nanoreactors with a merocyanine photoacid yielded a light-induced trigger. Loading the BCNs with HRP resulted in light-responsive enzymatic conversion, with longer irradiation times corresponding to increased product formation. Furthermore, samples kept in the dark showed negligible conversion of the substrate. We were able to translate this behavior towards a hydrogel matrix in which the BCNs were immobilized. Similarly, the nanoreactors showed a light-induced permeability switch. We took advantage of the immobilized nanoreactors by selective irradiation of the hydrogel using a photomask, which resulted in spatial control over permeability, as only illuminated areas showed conversion of the substrate. Higher spatiotemporal

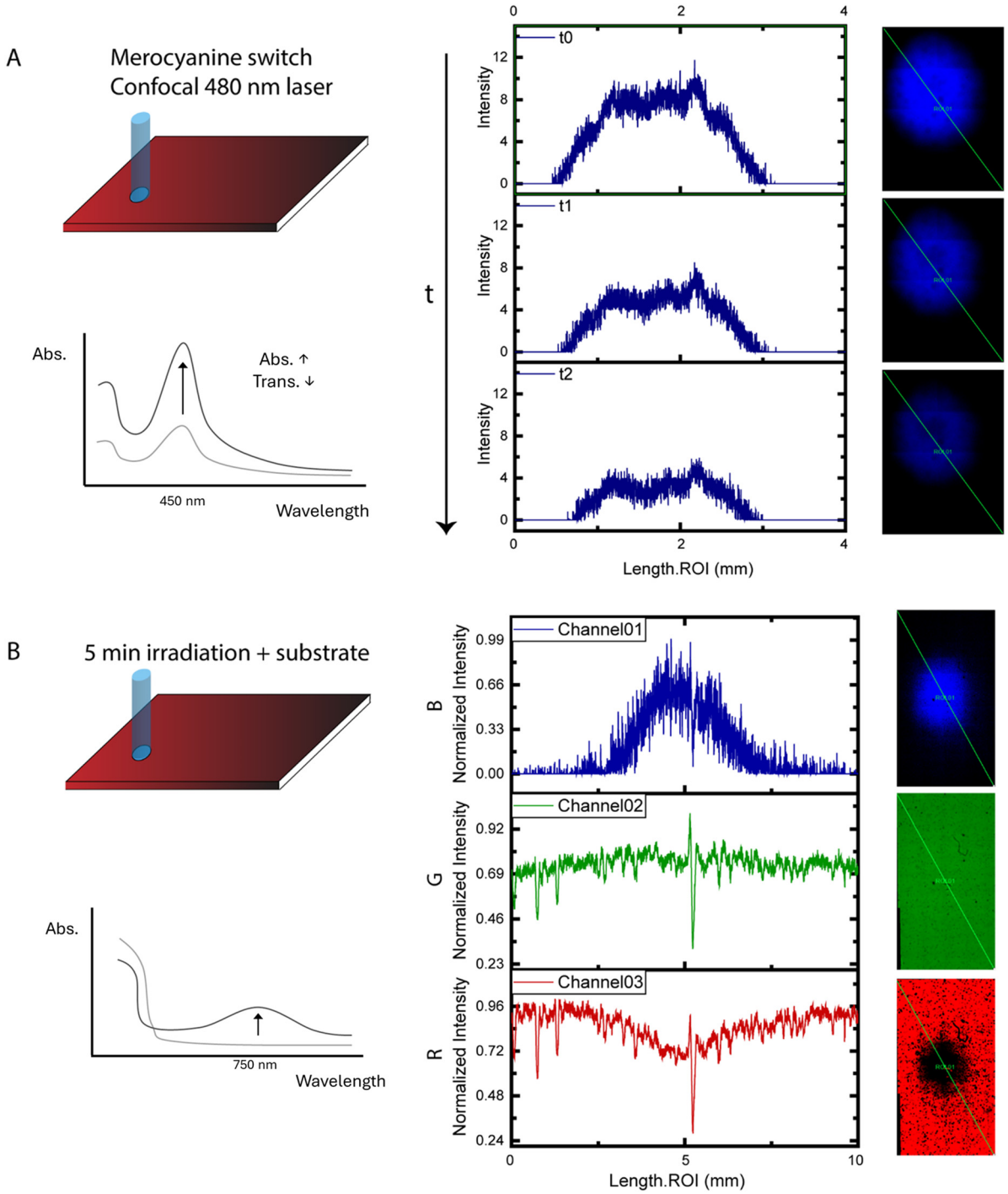

Fig. 6 Spatial control of permeability by confocal microscopy as determined by absorbance changes in the RGB channels. MCH is photoisomerized using the 480 nm laser line. (A) 1 min irradiation at 100% laser intensity switches MCH. Increased transmission due to decreased MCH absorbance results in an increased blue signal in the blue channel, which decreases over time due to MCH recovery and diffusion. (B) Confocal laser induced permeability switch. After 5 minutes of irradiation, the blue channel transmission is increased and red channel transmission is decreased, indicating spiropyran and $ABTS^{*+}$ formation, respectively. Contrast of channels is increased for visibility purposes.

resolution could be achieved with a confocal laser to switch the merocyanine. At the site of laser irradiation, we observed merocyanine isomerization to spiropyran, which rapidly relaxed over time, as well as the conversion of ABTS into $ABTS^{*+}$. This light-induced permeability switch could not only be used for the controlled synthesis of products but is also applicable for the release of encapsulated cargo, *i.e.* drugs or growth factors, in a spatiotemporally controlled manner. One could also envision the use of alternative photoacids or agents in the BCN-gel system in the future.

4. Experimental

4.1. Materials

All materials were used as received unless stated otherwise.

Horseradish peroxidase from *Amoracia rusticana* (Type VI, 295 U mg^{-1}), 4-methoxyphenylhydrazine hydrochloride (95%), isopropyl methyl ketone, 1,3-propanesultone (98%). 2-Hydroxybenzaldehyde, acrylamide, *N*,*N*′-methylene bisacrylamide, lithium phenyl-2,4,6-trimethylbenzoylphosphinate, 2,2′-azino-bis(3-ethylbenzothiazoline-6-sulfonic acid) diammonium salt (98%) were purchased from Sigma Aldrich. Polymer bicontinuous nanospheres were synthesized according to previously published procedures.[30]

4.2. Instruments

4.2.1. Nuclear magnetic resonance spectroscopy (NMR). ^{1}H NMR & ^{13}C NMR spectra were recorded on a Bruker (400 MHz, 100 MHz) spectrometer with DMSO-d6 as solvent unless stated otherwise.

4.2.2. UV-vis spectroscopy (UV-vis). Time-dependent UV-vis measurements were performed on a Cary 3500 UV-vis spectrophotometer. Merocyanine was irradiated at 405 nm, CoolLED pE-800 device, 5 mW cm^{-2}, at a distance of 10 cm.

4.2.3. Plate reader assays. Time-dependent absorbance of the hydrogels was measured on a Tecan™ Spark 10M plate reader using Corning Falcon 96 Black Flat Transparent well plates. Tecan™ Spark 10M has linear OD measurements between 0–4 OD. The hydrogels were prepared in these 96-well plates (100 μL volume).

4.2.4. UV photoreactor. The crosslinking of the nanoreactors and the polymerization of the hydrogels was performed using a Luzchem **LZC-4V** photoreactor equipped with 14 UVA lamps with a wavelength of 365 nm and power density of 5 mW cm^{-2}. Samples were placed at a distance of 15 cm.

4.2.5. Confocal laser scanning microscopy (CLSM). Microscopy imaging of samples was performed on a Leica SP8 inverted microscope with a 10× dry objective (HC PL APO CS2 10×/0.40 Dry). Samples were sandwiched between two microscopy 1.5 coverslips and imaged before and after irradiation *via* an 8-bit digital camera Leica-DFC, 1920 × 1440 pixels at 40 MHz in RGB brightfield mode, with 1 ms exposure. Large areas of samples (>3 × 3 mm) were imaged *via* tile scanning. Prior irradiation was monitored over 2 min, at 0.722 s per frame. Conversion of merocyanine to the spiropyran was achieved by irradiating the approximate center of the tile scan in confocal mode using an argon laser at 480 nm at 512 × 512 600 Hz, at 10× zoom. No detectors were on during irradiation, and the irradiation time varied between 1 and 5 minutes.

4.3. Methods

Synthesis methods and characterization are described in the ESI.†

4.3.1. Assembly of HRP-loaded BCNs. 1 mg of HRP was dissolved in 1 mL MQ Ultrapure water in a 4 mL vial equipped with a magnetic stirrer rotating at 500 rpm. The block copolymer $mPEG_{45}$-*b*-p[$DEAEMA_{175}$-*co*-BMA_{28}] was dissolved in 1 mL THF to obtain a final concentration of 5 mg mL^{-1}. 1 mL polymer solution was added to 1 mL enzyme solution with a flowrate of 1 mL h^{-1} *via* a syringe pump. The cloudy suspension was immediately crosslinked by UV irradiation for 5 minutes at 5 mW cm^{-2} (Luzchem LZC-4V photoreactor equipped with 14 UVA lamps with a wavelength of 365 nm, distance of 15 cm) and transferred to a 12–14 kDa MWCO membrane and dialyzed against milliQ ultrapure water.

4.3.2. Synthesis of BCN loaded AAm hydrogels. 10 wt% acrylamide (AAm) hydrogel using *N*,*N*′-methylenebisacrylamide (MBA) as crosslinker (50 : 1 AAm : MBA) was synthesized using 1 mg mL^{-1} lithium phenyl-2,4,6-trimethylbenzoylphosphinate (LAP) as photoinitiator. The BCNs as well as 0.5 mM of merocyanine **1** were dispersed in the monomer solution prior to the photopolymerization step. The hydrogels were synthesized by dispersing 100 μL of the monomer solution into transparent 96-well plates prior to photopolymerization for 6 minutes using a UV chamber with a power of 5 mW cm^{-2} at λ = 365 nm.

A release/leakage assay was carried out to investigate any possible reduction in BCN entrapment amount over time. 100 μL gels with 25 μg mL^{-1} BCNs were prepared as described above, and immersed in 0.5 mL of water. The derived count rate from DLS was monitored in the supernatant, as an indication of BCN presence over 72 hours (Fig. S13, ESI†).

4.3.3. HRP activity assays. The influence of the photoacid and UV irradiation (and associated pH drop) on the HRP activity was investigated. Merocyanine was irradiated at 405 nm for 5 min, CoolLED pE-800 device, 5 mW cm^{-2}, at a distance of 10 cm. 0.1 μg mL^{-1} of HRP in 5 mM phosphate buffer (pH 7) was used for this study. The conversion of ABTS was followed over time by following the 415 nm absorbance using UV-vis plate reader and the slope was calculated as representative of the relative enzymatic activity between respective conditions. The results are illustrated in Fig. S12A and B (ESI†). The concentrations of ABTS and H_2O_2 were the same for all conditions, 2 mM and 1 mM respectively.

Author contributions

The manuscript was written through contributions of all authors. All authors have approved the final version of the manuscript.

Data availability

The data supporting this article have been included as part of the ESI.†

Conflicts of interest

There are no conflicts to declare.

Acknowledgements

The authors thank the NWO TA program Soft Advanced Materials'' (741.018.202), the Spinoza premium SPI 72-259 and the gravitation program Interactive Polymer Materials, 024.005.020, for financial support.

References

1 A. Walther, Viewpoint: From Responsive to Adaptive and Interactive Materials and Materials Systems: A Roadmap, *Adv. Mater.*, 2020, **32**, 1905111, DOI: **10.1002/adma.201905111**.

2 M. M. Lerch, A. Grinthal and J. Aizenberg, Viewpoint: Homeostasis as Inspiration—Toward Interactive Materials, *Adv. Mater.*, 2020, **32**, 1905554, DOI: **10.1002/adma.201905554**.

3 J. Boekhoven, W. E. Hendriksen, G. J. M. Koper, R. Eelkema and J. H. Van Esch, Transient Assembly of Active Materials Fueled by a Chemical Reaction, *Science*, 2015, **349**, 1075–1079, DOI: **10.1126/science.aac6103**.

4 B. Rieß, R. K. Grötsch and J. Boekhoven, The Design of Dissipative Molecular Assemblies Driven by Chemical Reaction Cycles, *Chem*, 2020, 552–578, DOI: **10.1016/j.chempr.2019.11.008**.

5 C. Sharma, I. Maity and A. Walther, PH-Feedback Systems to Program Autonomous Self-Assembly and Material Lifecycles, *Chem. Commun.*, 2023, **59**(9), 1125–1144, DOI: **10.1039/d2cc06402b**.

6 G. Fusi, D. Del Giudice, O. Skarsetz, S. Di Stefano and A. Walther, Autonomous Soft Robots Empowered by Chemical Reaction Networks, *Adv. Mater.*, 2023, **35**, 2209870, DOI: **10.1002/adma.202209870**.

7 X. Fan and A. Walther, Autonomous Transient PH Flips Shaped by Layered Compartmentalization of Antagonistic Enzymatic Reactions, *Angew. Chem., Int. Ed.*, 2021, **60**(7), 3619–3624, DOI: **10.1002/anie.202009542**.

8 A. E. Mangubat-Medina and Z. T. Ball, Triggering Biological Processes: Methods and Applications of Photocaged Peptides and Proteins, *Chem. Soc. Rev.*, 2021, 10403–10421, DOI: **10.1039/d0cs01434f**.

9 T. Slanina, P. Shrestha, E. Palao, D. Kand, J. A. Peterson, A. S. Dutton, N. Rubinstein, R. Weinstain, A. H. Winter and P. Klán, In Search of the Perfect Photocage: Structure-Reactivity Relationships in Meso-Methyl BODIPY Photoremovable Protecting Groups, *J. Am. Chem. Soc.*, 2017, **139**(42), 15168–15175, DOI: **10.1021/jacs.7b08532**.

10 Y. Li, M. Wang, F. Wang, S. Lu and X. Chen, Recent Progress in Studies of Photocages, *Smart Mol.*, 2023, **1**, e20220003, DOI: **10.1002/smo.20220003**.

11 J. Volarić, W. Szymanski, N. A. Simeth and B. L. Feringa, Molecular Photoswitches in Aqueous Environments, *Chem. Soc. Rev.*, 2021, 12377–12449, DOI: **10.1039/d0cs00547a**.

12 A. Goulet-Hanssens, F. Eisenreich and S. Hecht, Enlightening Materials with Photoswitches, *Adv. Mater.*, 2020, **32**, 1905966, DOI: **10.1002/adma.201905966**.

13 P. K. Kundu, S. Das, J. Ahrens and R. Klajn, Controlling the Lifetimes of Dynamic Nanoparticle Aggregates by Spiropyran Functionalization, *Nanoscale*, 2016, **8**(46), 19280–19286, DOI: **10.1039/c6nr05959g**.

14 R. Klajn, P. J. Wesson, K. J. M. Bishop and B. A. Grzybowski, Writing Self-Erasing Images Using Metastable Nanoparticle ''Inks'', *Angew. Chem., Int. Ed.*, 2009, **48**(38), 7035–7039, DOI: **10.1002/anie.200901119**.

15 M. J. Fuchter, On the Promise of Photopharmacology Using Photoswitches: A Medicinal Chemist's Perspective, *J. Med. Chem.*, 2020, 11436–11447, DOI: **10.1021/acs.jmedchem.0c00629**.

16 W. A. Velema, J. P. Van Der Berg, M. J. Hansen, W. Szymanski, A. J. M. Driessen and B. L. Feringa, Optical Control of Antibacterial Activity, *Nat. Chem.*, 2013, **5**(11), 924–928, DOI: **10.1038/nchem.1750**.

17 P. Kobauri, F. J. Dekker, W. Szymanski and B. L. Feringa, Rational Design in Photopharmacology with Molecular Photoswitches, *Angew. Chem., Int. Ed.*, 2023, **62**, e202300681, DOI: **10.1002/anie.202300681**.

18 X. Wang, J. Hu, G. Liu, J. Tian, H. Wang, M. Gong and S. Liu, Reversibly Switching Bilayer Permeability and Release Modules of Photochromic Polymersomes Stabilized by Cooperative Noncovalent Interactions, *J. Am. Chem. Soc.*, 2015, **137**(48), 15262–15275, DOI: **10.1021/jacs.5b10127**.

19 O. Rifaie-Graham, S. Ulrich, N. F. B. Galensowske, S. Balog, M. Chami, D. Rentsch, J. R. Hemmer, J. Read De Alaniz, L. F. Boesel and N. Bruns, Wavelength-Selective Light-Responsive DASA-Functionalized Polymersome Nanoreactors, *J. Am. Chem. Soc.*, 2018, **140**(25), 8027–8036, DOI: **10.1021/jacs.8b04511**.

20 L. Wimberger, J. André, J. E. Beves and R. Li, Basic-to-Acidic Reversible PH Switching with a Merocyanine Photoacid, *Chem. Commun.*, 2022, **5610**, 5610, DOI: **10.26434/chemrxiv-2022-wnts7**.

21 L. Wimberger, S. K. K. Prasad, M. D. Peeks, J. Andreásson, T. W. Schmidt and J. E. Beves, Large, Tunable, and Reversible PH Changes by Merocyanine Photoacids, *J. Am. Chem. Soc.*, 2021, **143**(49), 20758–20768, DOI: **10.1021/jacs.1c08810**.

22 C. Berton, D. M. Busiello, S. Zamuner, R. Scopelliti, F. Fadaei-Tirani, K. Severin and C. Pezzato, Light-switchable Buffers, *Angew. Chem., Int. Ed.*, 2021, **60**, 21737, DOI: **10.1002/anie.202109250**.

23 P. K. Kundu, D. Samanta, R. Leizrowice, B. Margulis, H. Zhao, M. Börner, T. Udayabhaskararao, D. Manna and R. Klajn, Light-Controlled Self-Assembly of Non-Photoresponsive Nanoparticles, *Nat. Chem.*, 2015, **7**(8), 646–652, DOI: **10.1038/nchem.2303**.

24 D. Samanta and R. Klajn, Aqueous Light-Controlled Self-Assembly of Nanoparticles. Adv, *Opt. Mater.*, 2016, **4**(9), 1373–1377, DOI: **10.1002/adom.201600364**.

25 N. Cissé and T. Kudernac, Light-Fuelled Self-Assembly of Cyclic Peptides into Supramolecular Tubules, *ChemSystemsChem*, 2020, **2**, e2000012, DOI: **10.1002/syst.202000012**.

26 J. Guo, H. Y. Zhang, Y. Zhou and Y. Liu, Light-Controlled Reversible Self-Assembly of Nanorod Suprastructures,

Chem. Commun., 2017, **53**(45), 6089–6092, DOI: **10.1039/c7cc03280c**.

27 C. Maity, W. E. Hendriksen, J. H. Van Esch and R. Eelkema, Spatial Structuring of a Supramolecular Hydrogel by Using a Visible-Light Triggered Catalyst, *Angew. Chem., Int. Ed.*, 2015, **54**(3), 998–1001, DOI: **10.1002/anie.201409198**.

28 V. J. Périllat, E. Del Grosso, C. Berton, F. Ricci and C. Pezzato, Controlling DNA Nanodevices with Light-Switchable Buffers, *Chem. Commun.*, 2023, **59**, 2146–2149, DOI: **10.1039/D2CC06525H**.

29 S. Moreno, P. Sharan, J. Engelke, H. Gumz, S. Boye, U. Oertel, P. Wang, S. Banerjee, R. Klajn, B. Voit, A. Lederer and D. Appelhans, Light-Driven Proton Transfer for Cyclic and Temporal Switching of Enzymatic Nanoreactors, *Small*, 2020, **16**, 2002135, DOI: **10.1002/smll.202002135**.

30 W. P. van den Akker, H. Wu, P. L. W. Welzen, H. Friedrich, L. K. E. A. Abdelmohsen, R. A. T. M. van Benthem, I. K. Voets and J. C. M. van Hest, Nonlinear Transient Permeability in PH-Responsive Bicontinuous Nanospheres, *J. Am. Chem. Soc.*, 2023, **145**(15), 8600–8608, DOI: **10.1021/jacs.3c01203**.